



HAL
open science

A silicon rectangular micro-orifice for gas flow measurement at moderate Reynolds numbers: design, fabrication and flow analyses

A. Amnache, M. Omri, L. Fréchette

► To cite this version:

A. Amnache, M. Omri, L. Fréchette. A silicon rectangular micro-orifice for gas flow measurement at moderate Reynolds numbers: design, fabrication and flow analyses. *Microfluidics and Nanofluidics*, 2018, 22 (6), 10.1007/s10404-018-2077-x . hal-01914280

HAL Id: hal-01914280

<https://hal.science/hal-01914280v1>

Submitted on 8 Nov 2018

HAL is a multi-disciplinary open access archive for the deposit and dissemination of scientific research documents, whether they are published or not. The documents may come from teaching and research institutions in France or abroad, or from public or private research centers.

L'archive ouverte pluridisciplinaire **HAL**, est destinée au dépôt et à la diffusion de documents scientifiques de niveau recherche, publiés ou non, émanant des établissements d'enseignement et de recherche français ou étrangers, des laboratoires publics ou privés.

A silicon rectangular micro-orifice for gas flow measurement at moderate Reynolds numbers: design, fabrication and flow analyses

A. Amnache^{1,2} · M. Omri³ · L. G. Fréchette^{1,2}

This work describes a micro-flowmeter for moderate flow rates of gases based on a differential pressure measurement. The micro-flowmeters consist of a microfabricated silicon–glass rectangular micro-orifice plate, with external pressure measurement. We experimentally evaluate the effects of geometrics parameters, Reynolds number and compressibility on the discharge coefficient. The paper examines a series of 13 rectangular micro-orifice sizes, with orifice hydraulic diameters ranging from 115 to 362 μm . The behavior of the discharge coefficient is presented for orifice Reynolds numbers ranging from 200 to 18000. Agreement is shown between the experimental and numerical results of the discharge coefficient. The micro-flowmeters measure moderate flow of air ranging from 1 to 106 mg/s. This demonstration implements a design method of micro-flowmeters that can be used in a broad range of microfluidic applications, such as microreactors and power MEMS.

Keywords Micro-orifice · Flowmeter · Discharge coefficient · Microfluidic · Flow rate

1 Introduction

Over the past decades, the range of microfluidic devices has continued to grow, including not only low Reynolds number bioMEMS, but also devices with higher Reynolds number gas flow such as microreactors (Wiles et al. 2011; Jensen 2017) and power MEMS (Dunn-Rankin et al. 2005; Fréchette 2015). This growth was accompanied by a significant development of adequate instrumentation. A key parameter is flow rate, which can be challenging to measure in microsystems. Microelectromechanical systems (MEMS) flow sensors have been implemented using thermal principles (Cubukcu et al. 2014; Xue and Yan 2012; Kuo et al. 2012) or non-thermal principles (Berberig et al. 1998; Bouwstra et al. 1990; Nguyen et al. 2015). Table 1 summarizes the major parameters of flow

measurement obtained by various authors. One of the simplest non-thermal sensing principles is based on differential pressure drop across a calibrated flow obstruction inside a channel, where the generated pressure difference is proportional to the flow rate. Compared to the thermal flow sensors, the differential pressure sensors have many advantages: (1) thermal insulation is not critical (Elwenspoek 1999), which is a big challenge in the miniature systems, (2) no electrical contact with the fluid, which indicates less corrosion and damage (Wang et al. 2009). However, the disadvantage of the flow sensors based on differential pressure is that they have less measurement sensitivity at low-velocity flow regimes, since pressure difference, ΔP , is proportional to the square of velocity (Svedin et al. 2003), as illustrated in Fig. 1. On the other hand, thermal flow sensors such as calorimetric flow sensors have a high sensitivity in the low-velocity regime, but saturates at high velocities when the thermal boundary layer thickness became dominant (Elwenspoek 1999). Therefore, thermal flow sensors are more popular in microfluidic devices handling low velocity flow regimes and low Reynolds numbers, such as liquid flows in biochemical applications. However, with the appearance of microfluidic systems handling relatively high fluid pressure and flow rate such as micro-steam turbines, i.e., up 4.5 bars and 100 mg/s ($100 < Re < 2000$) (Lee and Fréchette 2011; Liamini et al. 2011), the differential pressure approach become of interest. Commercial flowmeters can measure the

✉ A. Amnache
amrid.amnache@usherbrooke.ca

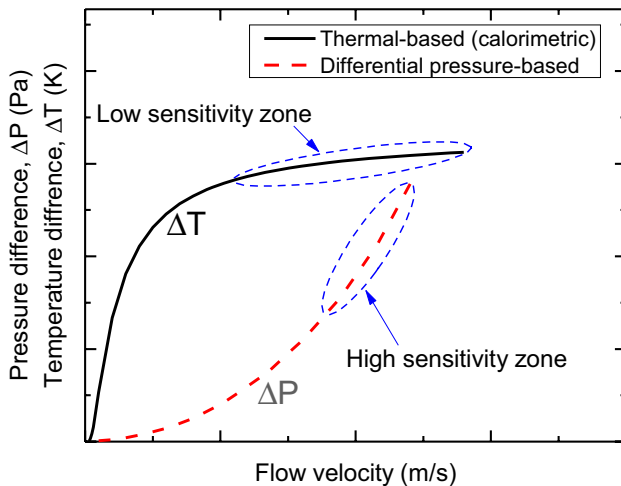
¹ Institut Interdisciplinaire d'Innovation Technologique (3IT), Université de Sherbrooke, 3000 boul. de l'Université, Sherbrooke, QC J1K 0A5, Canada

² Laboratoire Nanotechnologies Nanosystèmes (LN2), CNRS UMI-3463, Université de Sherbrooke, 3000 boul. de l'Université, Sherbrooke, QC J1K 0A5, Canada

³ King Abdulaziz University, Deanship of Scientific Research, Jeddah 21589, Kingdom of Saudi Arabia

Table 1 Major parameters of MEMS-based flow sensor for gas flow measurement

References	Working principle	Gas	Flow range	Chip dimension Sensor size
Xue and Yan (2012)	Thermal (calorimetric)	Air	0.016–57 mg/s	20×10×1.6 mm ³ No data
Cubukcu et al. (2014)	Thermal (calorimetric)	Air, He, Ne, Ar	0.04–2 m/s	No data 1 mm diameter
Svedin et al. (2003)	Hybrid: thermal/pressure force (drag force/hot wire)	Air	Up to 1620 mg/s Up to 4.3 m/s	No data 3×3 mm ²
Bouwstra et al. (1990)	Resonating (vibration)	Air	0–0.2 mg/s 0–3 m/s	No data 600×200×21 μm ³
Berberig et al. (1998)	Differential pressure (capacitive)	Air	0–22 m/s	5×8×1.4 mm ³ No data
Nguyen et al. (2015)	Pressure force (capacitive)	Air	0–19.2 m/s	No data 5.5×5.5 mm ²
This work	Differential pressure	Air	0–106 mg/s 0–310 m/s	5×1 cm ² (10 different sensors) 207×125 μm ² to 3005×5102 μm ²

**Fig. 1** Measurement sensitivity of the thermal-based calorimetric versus differential pressure-based flowmeters

flow range of the micro-steam turbine. However, they cannot be integrated in situ, within a device. Also, the temperature of the steam flow (up to 250 °C) precludes the use of commercial flowmeters. Since the steam micro-turbine is essentially fabricated by deep etching and wafer bonding, the constriction differential pressure can be easily fabricated on the same chip and at the same time, without adding fabrication steps. In this paper, we focused on the gas flow measurement by differential pressure using an orifice micro-flowmeter. At macroscale, this flow measurement method is widely used. The discharge coefficient, C_d , defined as the ratio of the actual flow rate over the ideal flow rate, is an important design parameter for the orifice plate flowmeter. It has been exhaustively studied for circular geometries and high Reynolds numbers (Miller 1996; White

1999), which is characteristic for macroscale fluidic systems. However, few studies of the discharge coefficient have been performed at moderate Reynolds numbers (Hollingshead et al. 2011; Johansen 1930). Jankovski et al. (2008) developed a semiempirical correlation of C_d for an incompressible flow through a small circular orifice. They considered the effect of the orifice length on the C_d . The model was correlated and validated with numerical simulations and the experimental results from Hasegawa et al. (2009), Phares et al. (2005) and Kiljanski (1993) for orifice Reynolds numbers up to 3000. However, micro-orifices fabricated with microfabrication processes are usually non-circular in cross section and take two-dimensional extruded-like shapes. Unfortunately, the traditional C_d correlations for circular orifices are not valid for rectangular or planar shapes (Amnache et al. 2010). It is therefore very desirable to study the discharge coefficient behavior in rectangular micro-orifices. Zivkovic et al. (2013) studied numerically the pressure drop of an incompressible flow across a rectangular micro-orifice. Their study developed a correlation between the loss coefficient as a function of orifice Reynolds number and geometry. However, the Reynolds number range was relatively low, from 0.005 to 0.1. Mishra and Peles (2005) fabricated rectangular micro-orifice plates entrenched in silicon microchannels for orifice hydraulic diameters between 21 and 57 μm. They experimentally studied the compressible and incompressible single-phase flow behavior through these configurations. They developed a correlation of the discharge coefficient for the incompressible flow and they concluded that the C_d depends only on the area ratio (orifice width/channel width) for Reynolds numbers greater than its critical value, ($200 \leq Re_{crit} \leq 500$). For compressible flow, the same authors determined the effect of the pressure ratio (upstream/downstream pressure) on the discharge coefficient.

They observed that for pressure ratios greater than 2, which corresponds to choked flow, i.e., Mach number equal to unity, the discharge coefficient becomes a constant value. However, the evolution of the discharge coefficient below pressure ratios of 2 was not well characterized. In addition, for both compressible and incompressible flows, the effect of the aspect ratio on the discharge coefficient was not considered. Amnache et al. (2010) numerically studied the gas flow through a rectangular micro-orifice and observed that the discharge coefficient strongly depends on the orifice aspect ratio.

In this paper, we design, fabricate and characterize rectangular orifice micro-flowmeters for measuring moderate gas flow. The design of this type of micro-flowmeter is based mainly on the knowledge of the discharge coefficient. However, the above brief literature survey shows that the discharge coefficient for compressible flow through micro-orifices with rectangular cross section has not been well studied. In this work, we endeavored to study numerically and experimentally the compressible gas flow through rectangular micro-orifices of various sizes, below the sonic limit. The discharge coefficient is characterized showing the effect of the Reynolds number, all the geometric parameters (orifice aspect ratio, area ratio, orifice length-to-hydraulic ratio) and compressibility.

This work provides a design methodology for microfabricated differential pressure flowmeters to allow their integration into embedded microfluidic devices that cannot use commercial flowmeters.

2 Rectangular orifice micro-flowmeter approach

Rectangular orifice micro-flowmeters are based on the Bernoulli obstruction theory. The orifice restriction as shown in Fig. 2 creates a Venturi effect, where the flow velocity increased to its maximum and the static pressure decreased to its minimum value at point 2, which corresponds to the *vena contracta*. The static pressure profile along the orifice micro-flowmeter is also illustrated in Fig. 2. It is a combination of the total pressure drop (Moody and head losses) and the dynamic pressure (Bernoulli effect).

By measuring pressure difference, $\Delta P = P_1 - P_2$, between the pressure tap 1 and the pressure tap 2, the velocity of the flow can be determined, leading to the ideal mass flow rate, \dot{m}_{id} .

For an isentropic unidimensional compressible flow through a channel (Shapiro 1953):

$$\frac{T_0}{T} = 1 + \frac{k-1}{2} M^2, \quad (1)$$

$$\frac{P_0}{P} = \left[1 + \frac{k-1}{2} M^2 \right]^{\frac{k}{k-1}}, \quad (2)$$

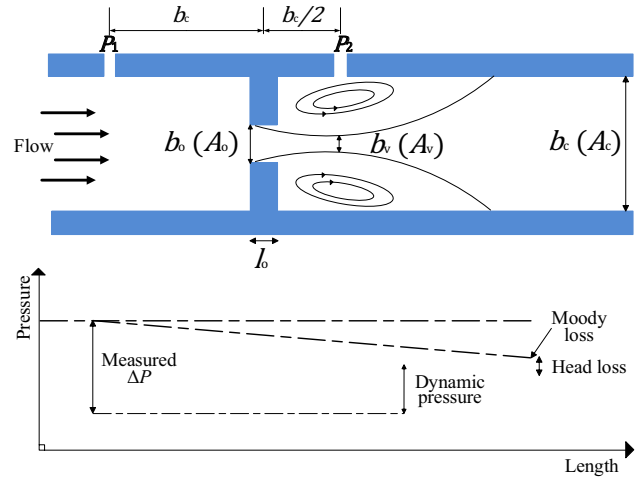


Fig. 2 Schematic diagram of the orifice flowmeter measurement approach

$$\frac{\rho_0}{\rho} = \left[1 + \frac{k-1}{2} M^2 \right]^{\frac{1}{k-1}}, \quad (3)$$

where P , T , and ρ are static pressure, static temperature and static density of the fluid. P_0 , T_0 and ρ_0 are, respectively, the total pressure, total temperature and total density. These relations are expressed as a function of Mach number, M , and depend on k , the specific heat ratio, which is equal to 1.4 for air.

The equation of state of an ideal gas is written as:

$$\frac{P}{\rho} = RT, \quad (4)$$

where R is the ideal gas constant, equal to 287 J/kg K for air.

Assuming an ideal case with no losses between upstream (1) and downstream (2) of the orifice, the ideal static pressure ratio can be given by:

$$\frac{P_1}{P_2} = \left[\frac{1 + \frac{k-1}{2} M_2^2}{1 + \frac{k-1}{2} M_1^2} \right]^{\frac{k}{k-1}}. \quad (5)$$

Assuming that the cross-sectional area of the *vena contracta*, A_v , is equal to the cross-sectional area of the orifice, A_o , and from mass conservation, the ratio A_o/A_c can be expressed as:

$$\frac{A_o}{A_c} = \left[\frac{1 + \frac{k-1}{2} M_2^2}{1 + \frac{k-1}{2} M_1^2} \right]^{\frac{k+1}{2(k-1)}}. \quad (6)$$

Replacing the Mach number, M_1 , calculated from Eq. 5, in Eq. 6, the Mach number at the *vena contracta*, M_2 , can be determined by:

$$M_2^2 = \frac{1 - \left(\frac{P_1}{P_2}\right)^{\frac{k}{k-1}}}{\frac{k-1}{2} \left(\frac{P_1}{P_2}\right)^{\frac{k}{k-1}} \left(\frac{A_o}{A_c \left(\frac{P_1}{P_2}\right)^{\frac{k}{k-1}}}\right)^2 - \frac{k-1}{2}}. \quad (7)$$

The ideal mass flow rate across the orifice can be obtained by (Shapiro 1953):

$$\dot{m}_{id} = \rho_2 A_o M_2 \sqrt{k R T_2}. \quad (8)$$

To express the mass flow rate as a function of the pressure difference between upstream and downstream of the orifice, the Mach number, M_2 , is replaced by Eq. 7 and the density, ρ_2 , is replaced by:

$$\rho_2 = \frac{\rho_1}{\left[1 + \frac{k-1}{2} M_2^2\right]^{\frac{1}{k-1}}}. \quad (9)$$

Then after rearrangement, the ideal mass flow rate can be expressed by:

$$\dot{m}_{id} = Y \frac{1}{\sqrt{1 - \beta^4}} A_o \sqrt{2 \rho_1 \Delta P}, \quad (10)$$

where β is the area ratio defined as the square root of the ratio of the orifice cross-sectional area, A_o , to the channel cross-sectional area, A_c , as:

$$\beta = \sqrt{\frac{A_o}{A_c}} \quad (11)$$

and Y is the expansion factor expressed for an adiabatic gas as:

$$Y = \left\{ \frac{\left(\frac{P_2}{P_1}\right)^{\frac{2}{k}} (1 - \beta^4) \left(\frac{k}{k-1}\right) \left[1 - \left(\frac{P_2}{P_1}\right)^{\frac{k}{k-1}}\right]}{\left[1 - \left(\beta^4 \left(\frac{P_2}{P_1}\right)^{\frac{2}{k}}\right)\right] \left(1 - \frac{P_2}{P_1}\right)} \right\}^{0.5}. \quad (12)$$

The expansion factor, Y , describes the effect of compressibility. Indeed, if the pressure difference across the orifice is small, the expansion factor, Y , tends to unity. It results in no significant change in density of the gas and then the flow can be assumed incompressible.

In the actual case, there will be a total pressure drop across the orifice due to friction losses. Also, the section of the *vena contracta* at point 2 will not necessarily be equal to the orifice cross-sectional area. The ideal mass flow rate is therefore typically corrected by the discharge coefficient,

C_d , which must be determined for a given geometry and flow conditions to account for these non-idealities. So, the actual mass flow rate, \dot{m} , can be written as:

$$\dot{m} = C_d Y \frac{1}{\sqrt{1 - \beta^4}} A_o \sqrt{2 \rho_1 \Delta P}. \quad (13)$$

Unlike the traditional circular orifice plate, the discharge coefficient is expected to depend on three geometric parameters: area ratio, β , orifice aspect ratio, δ , defined as the ratio of the orifice width, b_o , over the channel depth, ω :

$$\delta = \frac{\omega}{b_o} \quad (14)$$

and orifice length-to-hydraulic diameter ratio, λ , defined as the ratio of the orifice length, l_o , over its hydraulic diameter, dh_o :

$$\lambda = \frac{l_o}{dh_o}, \quad (15)$$

where dh_o is defined as:

$$dh_o = \frac{2b_o\omega}{b_o + \omega}. \quad (16)$$

3 Design and microfabrication of rectangular orifice micro-flowmeters

A series of 13 rectangular orifice micro-flowmeters are designed with different geometries. To study the influence of the geometric parameters on the discharge coefficient, each micro-flowmeter geometry is defined by three dimensionless parameters: the area ratio, β , the orifice aspect ratio, δ , and the orifice length-to-hydraulic diameter ratio, λ . The dimensions and parameters of the micro-flowmeters are presented in Table 2.

Localization of pressure taps for measuring average static pressure upstream, P_1 , and downstream, P_2 , of the orifice are designed to be in agreement with the American Society of Mechanical Engineers standardization at macroscale (Miller 1996). Namely the upstream pressure and downstream pressure taps are located at $-b_c$, $b_c/2$, respectively from the orifice. Amnache et al. (2010) found these locations to be appropriate for rectangular orifice micro-flowmeters.

The fabrication process flow for rectangular orifice micro-flowmeters is schematically illustrated in Fig. 3. The micro-devices are fabricated using silicon-on-insulator (SOI) wafer (100 mm, p-type, double side polished, 200 μm device layer, 300 μm handle layer and 200 nm silicon dioxide). After photolithography on the device layer using photoresist, channels, orifices and the pressure taps were formed by deep reactive ion etching (DRIE). DRIE gives re-entrant profiles when

Table 2 Summary of fabricated micro-flowmeters dimensions

Devices	β	δ	λ	b_c (μm)	b_o (μm)	ω (μm)	l_o (μm)	dh_o (μm)
1	0.2	1.7	3.9	3005	120	207	595	152
2	0.2	2.6	3.4	205	80	207	395	115
3	0.41	0.7	1.5	1890	310	207	370	248
4	0.4	1	1.2	1260	205	207	245	206
5	0.4	1.7	1	760	120	207	145	152
6	0.4	2.6	0.8	510	80	207	95	115
7	0.6	0.2	1.6	2787	1007	207	560	343
8	0.6	1	0.5	565	205	207	105	206
9	0.61	2.3	0.4	245	90	207	45	126
10	0.8	0.15	1.3	2270	1455	207	470	362
11	0.8	0.3	0.6	943	605	207	180	309
12	0.8	1.3	0.2	253	160	207	45	181
13	0.8	2.6	0.2	125	80	207	20	115

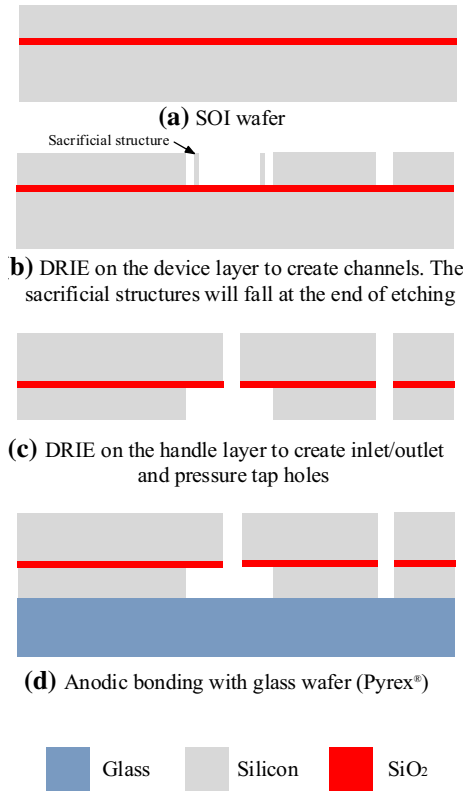


Fig. 3 Microfabrication process flow of rectangular orifice micro-flowmeters

etching trenches are larger than $50 \mu\text{m}$. However, verticality is important to have well-defined orifices and reproducible micro-flowmeters. To fabricate vertical channel walls, sacrificial structures were created near the wall, as represented in Fig. 3b, to create narrow trenches with vertical side walls. The width of the trench opening near the wall is $10 \mu\text{m}$. These sacrificial structures fall when the silicon dioxide layer is reached

due to under-etching on the side with a wider opening. The other requirement for reproducible results is control of the channel depth. Given the high selectivity with silicon dioxide, well controlled and uniform channel depth independent of the trench aspect ratio is achieved. Therefore, the depth of the all micro-flowmeters is defined by the SOI's device layer, measured here to be $207 \mu\text{m}$, with an uncertainty of 2.5%. The relative roughness of micro-channels (ratio of the average height of surface irregularities to the hydraulic diameter of the channel) is measured to be about 0.001 to 0.004.

Figure 4 shows a scanning electron microscopy image of the micro-orifice edge and the downstream pressure tap for device #10. The width of the pressure tap is $30 \mu\text{m}$. The image shows good verticality of the wall after DRIE. Another photolithography and DRIE process was performed on the handle layer of the SOI wafer etching holes of $400 \mu\text{m}$ diameter through $300 \mu\text{m}$ of Si in order to create the fluid inlet/outlet and pressure tap connections (Fig. 3c). Prior to bonding, the silicon wafer was cleaned with SC1 solution (1:1:5 mixture of $\text{NH}_4\text{OH}:\text{H}_2\text{O}_2:\text{H}_2\text{O}$) for 15 min. The wafer was also immersed in a hydrofluoric acid solution (1:50 mixture of $\text{HF}:\text{H}_2\text{O}$) for 30 s in order to remove the native oxide. To complete the micro-channels, the silicon wafer was anodically bonded to a Pyrex® glass wafer ($500 \mu\text{m}$ thickness), which is a good material choice for bond quality with silicon and to allow flow visualization in future studies (Fig. 3d). Finally, the wafer was diced into $5 \times 1 \text{ cm}$ rectangular chips with multiple flowmeters, as illustrated in Fig. 5. Distances between fluid inlet/outlet and the center of the orifice are 5.5 and 3.5 mm, respectively.

4 Experimental apparatus and procedure

A schematic of the experimental setup is represented in Fig. 6. In the current study, extra dry air ($\text{H}_2\text{O} < 10 \text{ ppm}$) is used as the working fluid. The chip of micro-flowmeters is

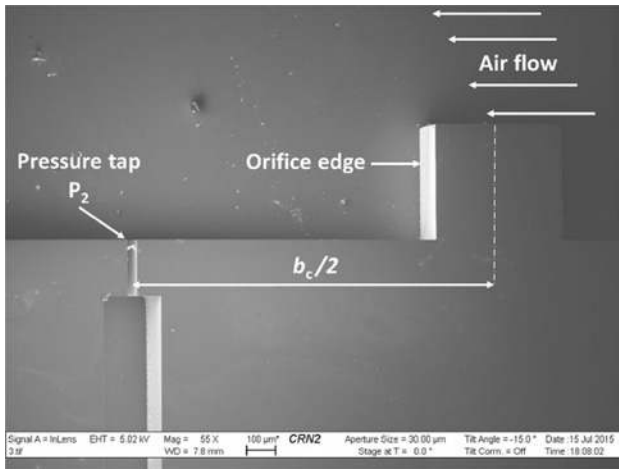


Fig. 4 Scanning electron microscopy image showing orifice and pressure tap P_2 of the device #10. The air flows from right to left

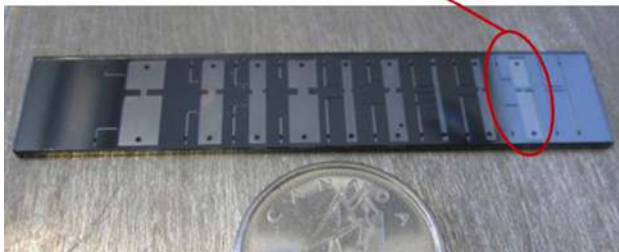
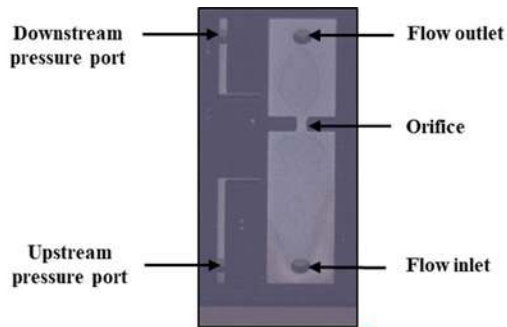


Fig. 5 A photograph of the chip with multiple micro-flowmeters. Length, 5 cm; width, 1 cm; thickness, 1 mm

embedded in a packaging designed specifically for this, as shown in Fig. 7. It is made of three layers of stainless steel. Layer A consists of fluidic piping and O-ring grooves. The connections between the ports on the chip and layer A (inlet, outlet and pressure taps) are provided using micro O-rings made of Markez perfluoroelastomer (inner diameter and cross section of $600\ \mu\text{m}$). Layer B is designed to hold and align the micro-flowmeter chip in the middle of layer C and it serves as a mechanical stop when the O-rings are squeezed by both layers A and C. The inlet to the micro-flowmeters is connected to an air source, where the pressure is be adjusted

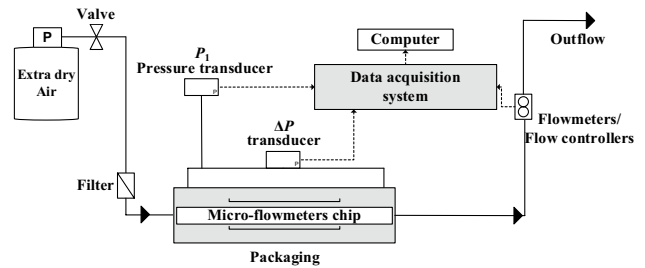


Fig. 6 Experimental setup schematic

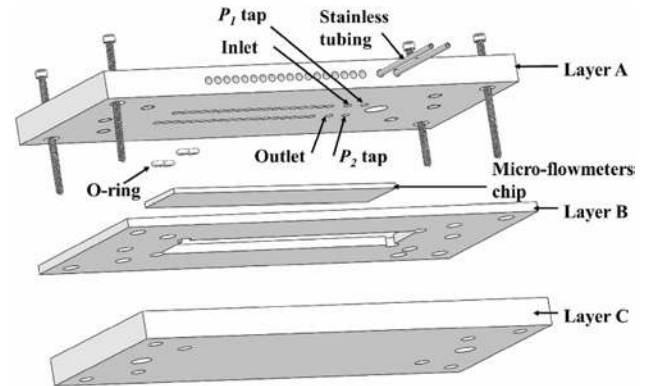


Fig. 7 Exploded schematic view of the micro-flowmeters packaging

by a pressure regulator. The air is filtered before passing through the micro-flowmeters. The differential pressure between inlet and outlet of micro-orifices is measured by a differential pressure transducer (Scanivalve[®] Zoc17IP/8PX-APC) capable of pressure differences up to 700 kPa with an uncertainty of 0.455 kPa. The upstream pressure P_1 is measured separately by a simple pressure transducer (Omega[®]) capable to measure pressure up to 1 MPa with an uncertainty of 2.5 kPa. The reason to measure P_1 is to calculate the density of the air at this location using Eq. 4, assuming room temperature. In this experiment, we used mass flow controllers to control the mass flow rate with an uncertainty of 1% of full scale (MKS[®] 1179A). Since we studied a large range of mass flow rates, we used three different mass flow controllers having different measurement ranges (0–200, 0–500 and 0–5000 sccm) to increase the precision of measurement. Finally, pressure and mass flow rate data were collected through a data acquisition and control (DAQ) system.

5 Results and discussion

The characteristics of the flow through the rectangular orifice plate micro-flowmeter have been evaluated experimentally for the 13 different sizes and over a range of operating conditions. The air at ambient temperature is used for these

experiments. The results show the pressure difference across micro-flowmeter, and the effect of geometry, Reynolds number and compressibility on the discharge coefficient. Furthermore, the numerical simulations are validated by the experimental results.

5.1 Pressure difference across micro-orifices

The pressure difference, ΔP , across micro-orifices is measured by varying mass flow rate within the range of 1–106 mg/s. The upstream pressure, P_1 , is maintained at 0.8 MPa. Figure 8 shows the behavior of ΔP versus the mass flow rate for each micro-flowmeter. The ΔP increases quadratically as mass flow rate increases. As discussed previously, the results show that orifice micro-flowmeters have a high sensitivity at high flow rate. Furthermore, the results revealed that a high orifice aspect ratio gives a high pressure difference when the area ratio is fixed. Indeed, the depth of channels is constant (207 μm), so when the aspect ratio increases, orifice cross-sectional area decreases and then the dynamic pressure becomes more important. Therefore, the static pressure at the *vena contracta* decreases resulting in a larger pressure difference.

The maximum mass flow rate range in these measurements was limited by (Fig. 8):

- The mass flow controller limit (106 mg/s at $P_1 = 0.8$ MPa) as shown for devices #7, #10 and #11.
- The increase of the pressure losses inside the micro-channel (upstream and downstream of the orifice) and the canalizations as shown for #3 and #4.
- The critical flow where the Mach number reaches unity at the *vena contracta* as shown for #1, #2, #5, 6, #8, #9, #12 and #13. At this limit, the pressure differ-

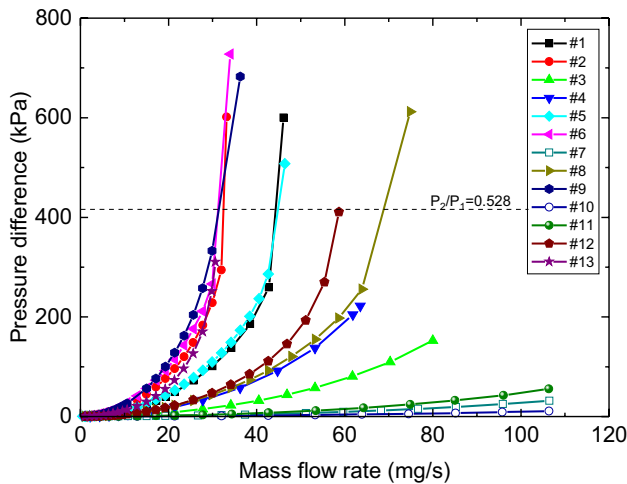


Fig. 8 Measured pressure difference across the orifices for various micro-flowmeters. The upstream pressure P_1 is maintained at 0.8 MPa

ence increased significantly due shock waves. It corresponds to the theoretical critical pressure ratio (P_2/P_1) as shown in Fig. 8. The range of interest in this work will therefore stay below critical flow.

The Knudsen number, which evaluates the effect of rarefaction on flow properties, was estimated by Eq. 17 (Morinin et al. 2004) to be an order of 10^{-5} , for the smallest device (#2). It is well below 10^{-3} , so the flow can be considered as a continuum:

$$Kn = \sqrt{\frac{\pi k}{2}} \frac{M_2}{Re_o} \quad (17)$$

Re_o is orifice Reynolds number defined as:

$$Re_o = \frac{\rho_o V_o d h_o}{\mu} = \frac{\dot{m} d h_o}{\mu A_o} \quad (18)$$

where ρ_o , V_o and μ are the fluid density, average velocity and viscosity at the orifice, respectively.

5.2 Discharge coefficient

5.2.1 Effect of geometric parameters

The discharge coefficient, Cd, of the flow through micro-orifices is plotted versus orifice aspect ratio and area ratio with varying orifice Reynolds number from 200 to 18,000. The uncertainty in the discharge coefficient comes from measurement error of the differential pressure transducer, flow controllers and dimensions of the micro-flowmeters.

As shown in Fig. 9, the general trend is a sharp increase in Cd from low Re_o to reach a nearly constant value above $Re_o \approx 3000$. This behavior is expected since the viscous losses diminish as Re_o increases, leading to a Cd closer to unity (ideal flow). At high Re_o , we observe that Cd increases again in some cases (such as micro-flowmeters #5, #6, #9, #12 and #13). Here, the fluid velocity and pressure difference become more important, so compressibility effect appears. To better confirm the role of compressibility, the Mach number at the *vena contracta*, M_2 , is estimated by Eq. 19 (Shapiro 1953) and added to Fig. 9. We notice indeed that Cd begins to increase again when M_2 reaches the range of 0.25–0.4.

$$\frac{P_2}{P_1} = \left[\frac{k-1}{2} M_2^2 + 1 \right]^{\frac{-k}{k-1}} \quad (19)$$

For micro-flowmeters #9, #12 and #13 the Cd behave differently at low Re_o . Indeed, the Cd increases a maximum near $Re_o \approx 2000$, after which it decreases to reach a constant value (before increasing again due to compressibility, as

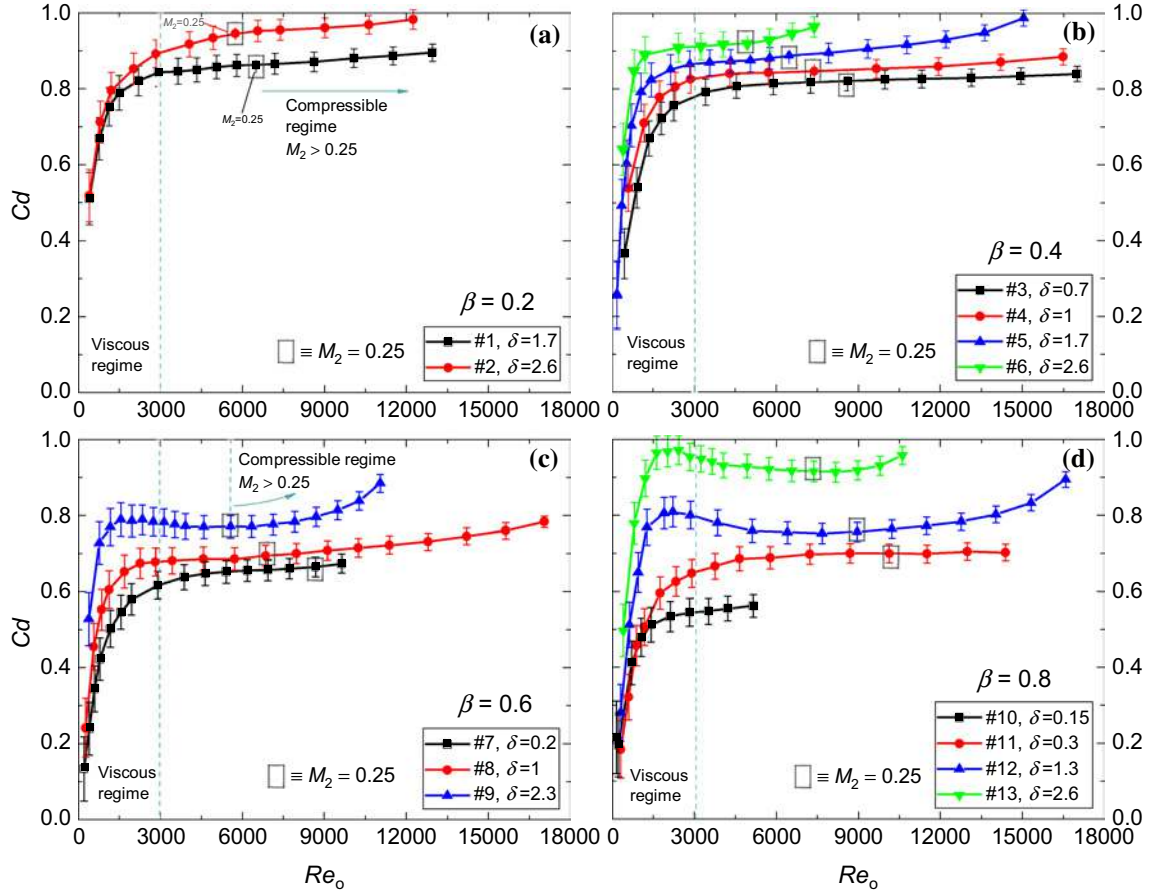


Fig. 9 Discharge coefficient plots with several area ratios. **a** $\beta=0.2$, **b** $\beta=0.4$, **c** $\beta=0.6$ and **d** $\beta=0.8$

presented previously). The same behavior has been observed by Hollingshead et al. (2011) for macroscale orifices with $\beta=0.5-0.7$. They observed that the trend of Cd presents a local maximum at $Re_o \approx 300$. They explained this by the effect of the orifice plate thickness on the velocity profile at the *vena contracta*. In addition, the results from Jankovski et al. (2008) for small circular orifices indicate that the Cd exhibits a maximum at low Re_o when the length-to-hydraulic diameter ratio, λ , tends to zero. This is in agreement with the present results. Indeed, compared to other micro-flowmeters, the #9, #12 and #13 have the smallest λ , 0.4, 0.2 and 0.2, respectively. This suggests that all three geometric parameters, β , δ , and λ , should be considered in micro-flowmeters.

For a fixed area ratio, β , and orifice length-to-hydraulic diameter ratio, λ , the higher aspect ratios, δ , give higher discharge coefficients. This may be due to the velocity gradient that is becoming larger at the wall with smaller aspect ratios, which leads to high friction losses.

We compared the effect of the area ratio, β , on the Cd by fixing the aspect ratio, δ , to 1 as illustrated in Fig. 10. The data revealed that a higher β gives higher Cd. This is an unexpected result if we consider that an abrupt sudden

contraction and sudden expansion tends to produce high friction losses. Furthermore, micro-flowmeter #4 has a higher λ , which increases the Moody losses. A plausible explanation

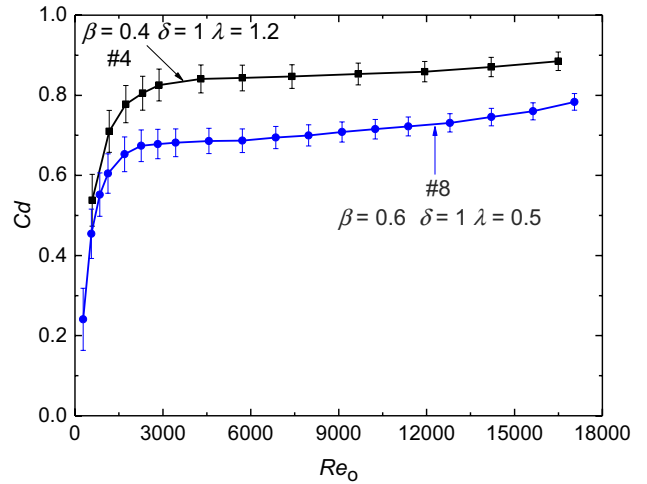


Fig. 10 Effect of area ratio, β , on the discharge coefficient, Cd. The aspect ratio, δ , is fixed at 1

is that the hypothesis taken in Eq. 6, mentioned that the area of the *vena contracta* is assumed equal to the area of the orifice, becomes invalid for rectangular orifice micro-flowmeters. Thus, the discharge coefficient determined in this study could be a combination of friction losses and *vena contracta* cross-sectional area deviation. To determine real friction losses through the orifice, the discharge coefficient should be divided by the contraction coefficient, C_c , defined as the ratio between the *vena contracta* and the orifice cross-sectional areas. However, numerical simulations or experimental flow visualization would be required to know the actual *vena contracta*.

5.2.2 Compressibility effect

The above results show that the C_d is affected by both Reynolds number and compressibility. In order to uncouple these two effects, we used 3D numerical simulation of the micro-flowmeter #4. Thus, ANSYS Fluent 14.5 is used to solve the compressible and incompressible steady-state Navier–Stokes equations. As the flow is symmetric, we calculated only a quarter of micro-flowmeter #8. Non-uniform hexahedral grids were used to mesh the geometry. The mesh is finer near the wall and orifice where the velocity gradients are larger. The meshed geometry contained 707,500 hexahedral cells. Inlet and outlet flow are situated at 3 mm upstream and 4 mm downstream, respectively, from the orifice. We used Reynolds stress model, RSM, to predict the transitional and turbulent flow through the orifice micro-flowmeter. Eiamsaard et al. (2008) observed that the prediction of the flow through a circular orifice with RSM is in agreement with measurements. Pressure-based solver and simple scheme are used to solve the discretized equations. The convergence criterion is satisfied when the residual of overall conservation equations reached 10^{-12} . The pressure drop across the orifice is evaluated by creating two surface planes at P_1 and P_2 taps location and calculating the average static pressure.

A comparison of experimental results and numerical simulations of the discharge coefficient is shown in Fig. 11. Two different series of numerical data as a function of Reynolds number are used. The first series has been performed using the same flow conditions as the experiment, i.e., compressible flow. The second series has been performed by simulating incompressible flow. The comparison revealed a good agreement of the experimental results with the numerical simulations taking into account the compressibility of the fluid. The deviation is less than 6%. On other hand, the numerical data for incompressible flow show concordance with the experimental results at low Re_o ranging from 2000 to 6000. This range of Re_o corresponds to M_2 ranging from 0.07 to 0.2. However, the deviation starts to become significant at $Re_o = 6800$. The related M_2 at this value is 0.25. Unlike the experimental measurement, the C_d

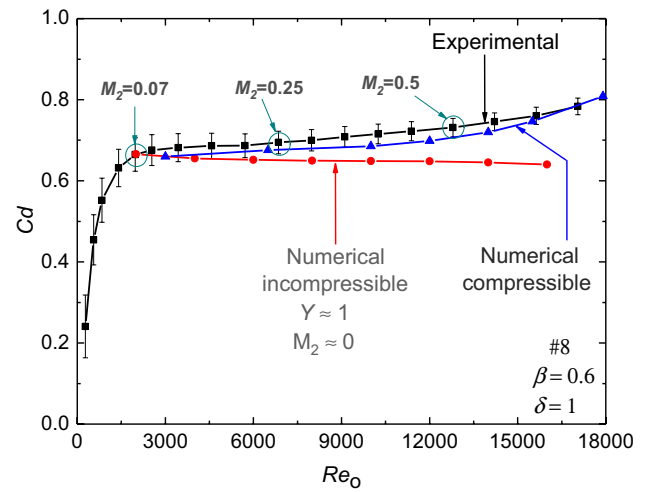


Fig. 11 Comparison of experimental results of the discharge coefficient with numerical simulations for both incompressible and compressible flow (micro-flowmeter #8)

remains constant with Re_o from 2000 to 16,000. This result confirms that the C_d is not only dependant on Re_o at high compressibility, but that the effect of Mach number should be considered.

6 Conclusion

In this work, a series of 13 non-traditional rectangular orifice micro-flowmeters have been fabricated successfully by MEMS fabrication methods. The air mass flow rate measured by these micro-flowmeters ranged from 1 to 106 mg/s.

The paper presents results concerning the behavior of the discharge coefficient in micro-flowmeters for Reynolds number ranging from 200 to 18,000. It was found that it is affected by orifice Reynolds number, compressibility, orifice aspect ratio, area ratio and orifice length-to-hydraulic diameter ratio.

We also found that the hypothesis used for circular orifices at macroscale mentioning an equality of the *vena contracta* and orifice cross-sectional areas may be not valid for rectangular micro-orifices and that it may be affected significantly by the area ratio and length-to-hydraulic diameter ratio. Consequently, the calculated discharge coefficients in this study do not present only friction losses through the orifice, but rather a combination of friction losses and the contraction coefficient. Further research work on the exact *vena contracta* cross-sectional area is recommended. The results in this work provide results allowing the design of simple micro-flowmeters for moderate Reynolds numbers, and can also be a guideline for further investigation of the flow through rectangular micro-orifices.

The agreement between the experimental and numerical results shows that numerical simulation using RSM model can serve as a good analysis tool for rectangular orifice micro-flowmeters, further opening the design options.

Acknowledgements The authors would like to thank Dr. Gholamreza Mirshekari for his technical contribution in cleanroom fabrication and methods. This work was supported by the NSERC and Canada Research Programs. The authors gratefully acknowledge this support.

References

- Amnache A, Omri M, Fr chet LG (2010) An analytical and numerical study of rectangular orifice plate microflowmeters. *ASME Int Mech Eng Congress Expos Proc* 10:659–665
- Berberig O, Nottmeyer K, Mizuno J, Kanai Y (1998) The Prandtl micro flow sensor (PMFS): a novel silicon diaphragm capacitive sensor for flow-velocity measurement. *Sens Actuators A Phys* 66:93–98
- Bouwstra S, Legtenberg R, Tilmans H, Elwenspoek M (1990) Resonating microbridge mass flow sensor. *Sens Actuators A Phys* 21:332–335
- Cubukcu AS, Romero DFR, Urban GA (2014) A dynamic thermal flow sensor for simultaneous measurement of thermal conductivity and flow velocity of gases. *Sens Actuators A Phys* 208:73–87
- Dunn-Rankin D, Martins Leal E, Walther DC (2005) Personal power systems. *Prog Energy Combust Sci* 31:422–465
- Eiamsa-ard S, Ridluan A, Somravysin P, Promvong P (2008) Numerical investigation of turbulent flow through a circular orifice. *KMITL Sci J* 8:43–50
- Elwenspoek M (1999) Thermal flow micro sensors. *Proc Int Semicond Conf* 2:423–435
- Fr chet LG (2015) Micro energy conversion devices. In: Li D (ed) *Encyclopedia of microfluidics and nanofluidics*. Springer, New York
- Hasegawa T, Ushida A, Narumi T (2009) Huge reduction in pressure drop of water, glycerol/water mixture, and aqueous solution of polyethylene oxide in high speed flows through micro-orifices. *Phys Fluids* 21:052002–052009
- Hollingshead CL, Johnson MC, Barfuss SL, Spall RE (2011) Discharge coefficient performance of Venturi, standard concentric orifice plate, V-cone and wedge flow meters at low Reynolds numbers. *J Pet Sci Eng* 78:559–566
- Jankovski TA, Schmierer EN, Prenger FC, Ashworth SP (2008) A series pressure drop representation for flow through orifice tubes. *J Fluids Eng* 130:51204-1-7
- Jensen KF (2017) Flow chemistry—microreaction technology comes of age. *AIChE J* 63:858–869
- Johansen FC (1930) Flow through pipe orifices at low Reynolds numbers. *Proc R Soc Lond* 126:231–245
- Kiljanski T (1993) Discharge coefficient for free jets from orifices at low Reynolds number. *Trans ASME J Fluids Eng* 115:778–781
- Kuo JTW, Yu L, Meng E (2012) Micromachined thermal flow sensors—a review. *Micromachines* 3:550–573
- Lee C, Fr chet LG (2011) A silicon microturbopump for a Rankine cycle power generation microsystem—part I: component and system design. *J Microelectromech Syst* 20:312–325
- Liamini M, Shahriar H, Vengallatore S, Fr chet LG (2011) Design methodology for a rankine microturbine: thermomechanical analysis and material selection. *J Microelectromech Syst* 20:339–351
- Miller RW (1996) *Flow measurement engineering handbook*, 3rd edn. McGraw-Hill, Boston
- Mishra C, Peles Y (2005) Incompressible and compressible flows through rectangular microorifices entrenched in silicon microchannels. *J Microelectromech Syst* 14:1000–1012
- Morinin GL, Spiga M, Tartarini P (2004) The rarefaction effect on the friction factor of gas flow in microchannels. *Superlattices Microstruct* 35:587–599
- Nguyen SD, Paprotny I, Wright PK, White RM (2015) MEMS capacitive flow sensor for natural gas pipelines. *Sens Actuators A Phys* 231:28–34
- Phares DJ, Smedley GT, Zhou J (2005) Laminar flow resistance in short microtubes. *Int J Heat Fluid Flow* 26:506–512
- Shapiro A (1953) *Dynamics and thermodynamics of compressible fluid flow*, 1st edn. Ronald Press Co, New York
- Svedin N, Kalvesten E, Stemme G (2003) A lift force sensor with integrated hot-chips for wide range flow measurements. *Sens Actuators A Phys* 109:120–130
- Wang YH, Chen CP, Chang CM, Lin CP, Lin CH, Fu LM, Lee CY (2009) MEMS-based gas flow sensors. *Microfluid Nanofluid* 6:333–346
- White FM (1999) *Fluid mechanics*, 4th edn. McGraw-Hill, Boston
- Wiles C, Watts P (2011) Recent advances in micro reaction technology. *Chem Commun* 47:6512–6535
- Xue N, Yan WP (2012) A silicon–glass-based microfabricated wide range thermal distribution gas flow meter. *Sens Actuators A Phys* 173:145–151
- Zivkovic V, Zerna P, Alwahabi ZT, Biggs MJ (2013) A pressure drop correlation for low Reynolds number Newtonian flows through a rectangular orifice in a similarly shaped micro-channel. *Chem Eng Res Des* 91:1–6